Energy Spectrum of Two-Dimensional Excitons in a Nonuniform Dielectric Medium

M. R. Molas, A. O. Slobodeniuk, K. Nogajewski, M. Bartos, Ł. Bala, A. Babiński, K. Watanabe, T. Taniguchi, C. Faugeras, and M. Potemski

Phys. Rev. Lett. **123**, 136801 — Published 23 September 2019

DOI: 10.1103/PhysRevLett.123.136801

Energy spectrum of two-dimensional excitons in a non-uniform dielectric medium

M. R. Molas,[1,2,*] A. O. Slobodeniuk,[1] K. Nogajewski,[1,2] M. Bartos,[1,3] Ł. Bala,[1,2] A. Babiński,[2] K. Watanabe,[4] T. Taniguchi,[4] C. Faugeras,[1] and M. Potemski[1,2,†]

[1] *Laboratoire National des Champs Magnétiques Intenses, CNRS-UGA-UPS-INSA-EMFL, 25, avenue des Martyrs, 38042 Grenoble, France*
[2] *Institute of Experimental Physics, Faculty of Physics, University of Warsaw, ul. Pasteura 5, 02-093 Warszawa, Poland*
[3] *Central European Institute of Technology, Brno University of Technology, Purkyňova 656/123, 61200 Brno, Czech Republic*
[4] *National Institute for Materials Science, 1-1 Namiki, Tsukuba 305-0044, Japan*

We demonstrate that, in monolayers (MLs) of semiconducting transition metal dichalcogenides, the *s*-type Rydberg series of excitonic states follows a simple energy ladder: $\epsilon_n = -Ry^*/(n+\delta)^2$, n=1,2,..., in which Ry^* is very close to the Rydberg energy scaled by the dielectric constant of the medium surrounding the ML and by the reduced effective electron-hole mass, whereas the ML polarizability is only accounted for by δ. This is justified by the analysis of experimental data on excitonic resonances, as extracted from magneto-optical measurements of a high-quality WSe_2 ML encapsulated in hexagonal boron nitride (hBN), and well reproduced with an analytically solvable Schrödinger equation when approximating the electron-hole potential in the form of a modified Kratzer potential. Applying our convention to other, $MoSe_2$, WS_2, MoS_2 MLs encapsulated in hBN, we estimate an apparent magnitude of δ for each of the studied structures. Intriguingly, δ is found to be close to zero for WSe_2 as well as for MoS_2 monolayers, what implies that the energy ladder of excitonic states in these two-dimensional structures resembles that of Rydberg states of a three-dimensional hydrogen atom.

Coulomb interaction in a non-uniform dielectric medium [1, 2], is one of the central points in investigations of large classes of nanoscale materials, such as graphene [3, 4], colloidal nanoplatelets [5], two-dimensional (2D) perovskites [6, 7], and other atomically thin crystals including their heterostructures [8]. This problem has been largely discussed in reference to investigations of excitons in monolayers (MLs) of semiconducting transition metal dichalcogenides (S-TMDs) [9–13]. Surprisingly, at first sight, the Rydberg series of *s*-type excitonic states in these 2D semiconductors, doesn't follow the model system of a 2D hydrogen atom [14–16], with its characteristic energy sequence, $\sim 1/(n-1/2)^2$, of states with a principal quantum number n. The main reason for that is a dielectric inhomogeneity of the 2D S-TMD structures, *i.e.*, MLs surrounded by alien dielectrics. At large electron-hole (*e*-*h*) distances, the Coulomb interaction scales with the dielectric response of the surrounding medium whereas it appears to be significantly weakened at short *e*-*h* distances by the usually stronger dielectric screening in the 2D plane. A common approach to account for the excitonic spectra of S-TMD MLs refers to the numerical solutions of the Schrödinger equation, in which the *e*-*h* attraction is approximated by the Rytova-Keldysh (RK) potential [1, 2]. However, it is only solvable numerically. A more phenomenological and intuitive approach, presented below, might be an optional solution to this problem.

In this Letter, we demonstrate that the energy spectrum, ϵ_n (n=1, 2,...), of Rydberg series of *s*-type excitonic states in S-TMD MLs may follow an energy ladder: $\epsilon_n = -Ry^*/(n+\delta)^2$. From magneto-optical investigations, we accurately establish that Ry^*=140.5 meV and δ=-0.083 for a WSe_2 ML encapsulated in hexagonal boron nitride (hBN). The $\epsilon_n = -Ry^*/(n+\delta)^2$ ansatz is well reproduced with an analytical approach in which the *e*-*h* potential is assumed to have the form of a modified Kratzer potential [17]. Here $Ry^* = Ry\frac{\mu}{\varepsilon^2 m_0}$ is the effective Rydberg energy, scaled by the dielectric constant ε of the surrounding hBN medium and the reduced *e*-*h* mass μ, where Ry=13.6 eV and m_0 is the free electron mass. Dispersion of Ry^* and δ parameters in different studied samples, WSe_2, $MoSe_2$, MoS_2, and WS_2 MLs encapsulated in hBN, is discussed and the reduced *e*-*h* masses in these ML structures are estimated.

To accurately determine the characteristic ladder of *s*-type excitonic resonances in the experiment, we profited of a particularly suitable for this purpose method of magneto-optical spectroscopy [18, 19]. The active part of the structure used for these experiments was a WSe_2 ML embedded in between hBN layers. More details on samples' preparation and on the experimental techniques can be found in the Supplemental Materials (SM)[20]. We measured the (circular) polarization resolved magneto-photoluminescence (PL) at low temperatures (4.2 K) and in magnetic fields up to 14 T, applied in the direction perpendicular to the monolayer plane. Here we focus on magneto-PL spectra of our WSe_2 ML, observed in the spectral range from ∼1.7 to ∼1.9 eV. As shown in Fig. 1(a) and (b), these spectra are composed of up to five PL peaks, which are clearly resolved in the range of high magnetic fields. Following a number of previous investigations [24, 38–41] on similar structures, the observed PL peaks are identified with a series of excitonic

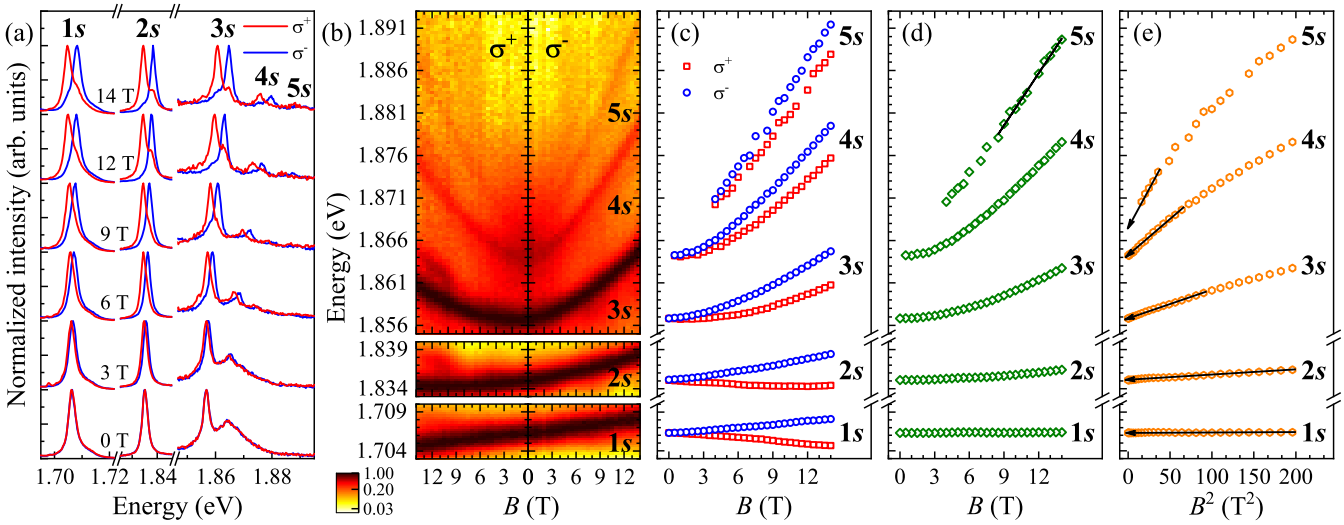

FIG. 1. (a) Helicity-resolved ($\sigma^{\pm}$) PL spectra of WSe_2 ML at selected magnetic fields. The separate parts of the spectra are normalized to the intensity of the 1s, 2s, and 3s lines. (b) False-colour map of the corresponding PL spectra from 0 to 14 T. (c) Obtained excitonic energies for $\sigma^{\pm}$ components as a function of magnetic fields. Mean energies of the $\sigma^{\pm}$ components of excitonic resonances measured on WSe_2 ML as a function of (d) B and (e) B^2. The black lines are obtained by fitting the presented data with (d) $E_{5s}(B) = A + 9/2\hbar\omega_c^*$ (A is a fitting parameter) and (e) $E_{ns}(B) = E_{ns}(B=0) + \sigma B^2$.

resonances forming the 1s, 2s, ..., 5s Rydberg series of the so-called A exciton [11, 12]. Each ns PL peak demonstrates the Zeeman effect. This is illustrated in Fig. 1(c) in which the energies of the $\sigma^{\pm}$-polarized PL peaks are plotted as a function of the magnetic field. In accordance with previous reports we extract g=-4.1 for g-factor of the 1s resonance, but read a significantly stronger Zeeman effect for all excited states (g ~-4.8). The later observation is intriguing and should be investigated in more details, which is, however, beyond the scope of the present paper. We have also carried out the magneto-PL experiments on MoS_2 and WS_2 monolayers encapsulated in hBN, but only the 1s and 2s resonances could be observed in these structures in the range of magnetic fields applied (see SM for details).

The magnetic field evolution of the mean energies of $\sigma^{\pm}$ PL peaks is illustrated in Figs 1(d) and (e). These energies, E_{ns}, are plotted as functions of the magnetic field B in Fig. 1(d), and its square B^2 in Fig. 1(e), which illustrate the characteristic behavior of ns states in the low- and high-field regime [14, 19]. The high field limit, for a given ns resonance, appears when $l_B \ll r_{ns}$, $E_b^{ns} \ll \hbar\omega_c^*/2$. Here r_{ns} and E_b^{ns} denote the root-mean-square radius and the binding energy E_b^{ns}=E_g-E_{ns} of a given ns state at B=0, $\hbar\omega_c^* = \hbar eB/\mu$, $l_B = \sqrt{\hbar/eB}$ is the magnetic length and other symbols have their conventional meaning. In the high-field limit, the energies of E_{ns} resonances approach a linear dependence upon B, with a slope given by $(n-1/2)\hbar\omega_c^*$. In the low field limit ($l_B \gg r_{ns}$, $E_b^{ns} \gg \hbar\omega_c^*/2$), the ns resonances display the diamagnetic shifts: $E_{ns}(B) = E_{ns}(B=0) + \sigma B^2$, with the diamagnetic coefficients $\sigma = (er_{ns})^2/8\mu$. The 1$s$ and 2s resonances follow the low-field regime in the entire range of the magnetic fields investigated due to their small exciton's radii and/or large binding energies, see Fig. 1(e). The high field regime is approached for the 5s resonances with an approximate linear dependence of E_{5s} with B, in the range above ~8 T. This dependence, marked with a solid line in Fig. 1(d), displays a slope of 2.1 meV/T, which if compared to $(9/2)\hbar\omega_c^*$ dependence, provides an estimate of 0.25 m_0 for the reduced mass in the WSe_2 ML. However, one may also argue that working with magnetic fields up to 14 T only, the high field limit is still barely developed even for the 5s state. In this context, our estimation of the reduced effective mass should be seen as its upper bound and, in the following we assume μ=0.2 m_0 for the WSe_2 ML, following the results of experiments performed in fields up to 60 T [24].

In the following we focus on the energy sequence E_{ns} of 1s, 2s, ..., 5s excitonic resonances as they appear in the absence of magnetic field. As shown in Fig. 1(e), the E_{ns} values are determined with linear extrapolations of E_{ns} versus B^2 dependences to B=0. Next, we assume that the sequence E_{ns} obeys the rule:

$$E_{ns} = E_g - Ry^*/(n+\delta)^2, \qquad (1)$$

where, at this point, E_g, Ry^*, and δ are regarded as adjustable parameters. To test the above formula against experimental data, we note that Eq. 1 implies that the ratio $(E_{3s} - E_{1s})/(E_{2s} - E_{1s})$ only depends on δ, and, reading it from the experiment, we extract δ=-0.083. With this value we find (see Fig. 2) that our experimental E_{ns} series perfectly matches Eq. 1 together with E_g=1.873 eV and Ry^*=140.5 meV (or exciton bind-

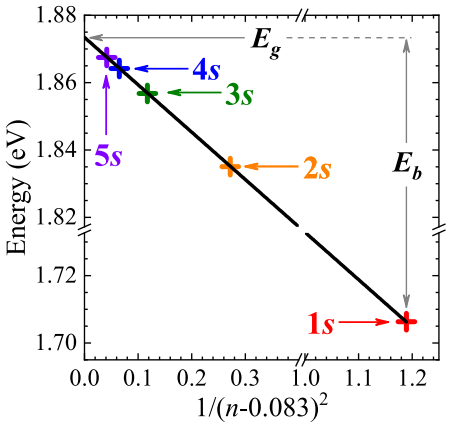

FIG. 2. Experimentally obtained transition energies for the exciton states as a function $1/(n+\delta)^2$ for δ=-0.083. The black line shows a fit of the data to the model described by Eq. 1. The grey lines denote the band-gap (E_g) and excitonic binding (E_b) energies.

ing energy $E_b = E_g - E_{1s}$ =167 meV). The above E_g and E_b values are in very good agreement with those already reported in the literature [24]. Relevant for our further analysis, is the observation that the derived value for Ry^* coincides well with the effective Rydberg energy Ry^*=13.6 eV$\cdot\mu/(\varepsilon^2 m_0)$=134.3 meV, scaled by the dielectric constant of the surrounding hBN material $\varepsilon = \varepsilon_{hBN}$=4.5 [27] and the reduced effective mass μ=0.2 m_0 [24] of the WSe_2 ML. Intriguingly, the extracted δ-parameter is close to zero which implies that the ϵ_n=E_{ns}-E_g Rydberg series found in a 2D system resembles that of a 3D hydrogen atom ($\epsilon_n \sim -1/n^2$).

On the theoretical ground, the problem of excitonic spectrum in S-TMD MLs is commonly solved by invoking the Rytova-Keldysh potential [1, 2] $U_{RK}(r)$ (purple curve in Fig. 3) to account for a specific character of the e-h attraction in these systems. At large e-h distances r, $U_{RK}(r)$ coincides with a usual Coulomb potential $U_{RK}(r) \sim -e^2/\varepsilon r$ (blue curve in Fig.3), which scales with the dielectric constant ε of the material surrounding the monolayer. On the other hand, $U_{RK}(r) \sim \log(r\varepsilon/r_0)$ when r is small, what accounts for the effective dielectric screening length $r_0 = 2\pi\chi_{2D}$ in the system, where χ_{2D} is the 2D polarizability of S-TMD ML. Distinctly, the apparent excitonic spectra and the related exciton binding energies critically depend on the efficiency of dielectric screening of the electron-hole attraction in the medium surrounding the monolayer.

Whereas previous efforts have been largely focused on the numerical study of such problem, we show that our model provides the analytical solution, which is in a good agreement with the experimental results discussed above. We propose to replace $U_{RK}(r)$ with the approximate potential $U_{app}(r)$, taken in the form of piecewise function. Namely, the sub-function $U_{cor}(r)$ defines $U_{app}(r)$ at small distances r (the core domain), while the external potential $U_{ext}(r)$ corresponds to $U_{app}(r)$ in the region outside of the core.

We choose the external potential in the form of the modified Kratzer potential [17] (given in CGS units)

$$U_{ext}(r) = -\frac{e^2}{r_0}\left[\frac{r_0^*}{r} - \frac{g^2 r_0^{*2}}{r^2}\right], \qquad (2)$$

where $r_0^* = r_0/\varepsilon$ is the reduced screening length and g is a tunable parameter. For the case of $g^2 = 0.21$, $U_{ext}(r)$ fits $U_{RK}(r)$ in the region $r > r_{min} = 0.46\, r_0^*$ with the relative deviation less than 5%. For the WSe_2 ML encapsulated in hBN, the distance $r_{min} = 4.6$ Å is comparable with the lattice constant $a = 3.28$ Å [42] of WSe_2 (see Fig 3 for comparison).

The Schrödinger equation with the Kratzer potential (2) provides the excitonic spectrum of the s-type states (see SM for details):

$$\epsilon_n = -Ry^*/(n + g\kappa - 1/2)^2, \qquad (3)$$

in which $\kappa^2 = 2r_0^*/a_B^*$ and $a_B^* = \hbar^2\varepsilon/\mu e^2$ is the effective Bohr radius. The effective Rydberg constant $Ry^* = e^2/2\varepsilon a_B^*$ sets the energy scale in the system, while $\delta = g\kappa - 1/2$ defines the relative positions of the energy levels in the spectrum. Note that Eq. 3 is an analogous of our experimentally found relation given by Eq. 1.

In the following, we introduce $U_{cor}(r)$, which replaces the Kratzer potential at small distances r, comparable with the lattice constant of WSe_2. We choose the constant attractive potential $U_{cor}(r) = V_0$. Below we demonstrate that it doesn't change $\propto (n+\delta)^{-2}$ behaviour of the spectrum and modifies only δ parameter.

We consider the Kratzer and constant potentials as external and core ones, respectively. We choose the parameter $g^2 = 0.21$ and the region of validity of the Kratzer potential up to its minimum $\xi_0 = 2g^2$, where $\xi = r/r_0^*$.

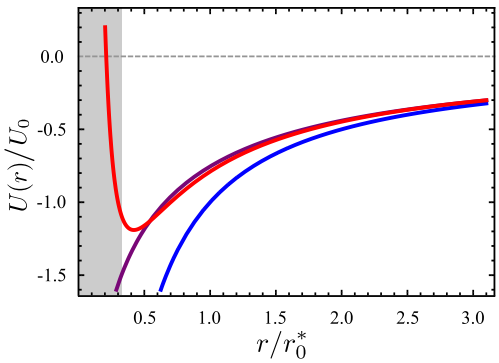

FIG. 3. Rytova-Keldysh (purple curve), Coulomb (blue curve) and Kratzer potential with $g^2 = 0.21$ (red curve), as a function of dimensionless parameter r/r_0^*. The energy scale is measured in units of $U_0 = e^2/r_0$. The grey rectangular depicts the region of distances smaller than the lattice constant $a = 3.28$ Å of WSe_2 ML encapsulated in hBN ($r_0^* = 10$ Å).

The parameter V_0 of the core potential is chosen as an average value of $U_{RK}(\xi)$ in the domain $\xi \in [0, \xi_0]$: $V_0 = 2\xi_0^{-2} \int_0^{\xi_0} d\xi \xi U_{RK}(\xi)$. Finally the approximate potential is

$$U_{app}(\xi) = -U_0 \Big\{ \Big[\frac{1}{\xi} - \frac{0.21}{\xi^2} \Big] \theta(\xi - \xi_0) + v_0\, \theta(\xi_0 - \xi) \Big\}, \quad (4)$$

where $\theta(x)$ is the step-function and $v_0 = 1.71134$. Note that the truncated Kratzer potential is applicable only if the radius of the core potential r_{cor} is less or comparable with the lattice constant a. We estimate that this requirement is well satisfied for all monolayers encapsulated in hBN, and in particular for our WSe_2 structure.Considering the s-type excitonic states in this later system, we derive the following formula (a detailed description is given in SM)

$$\epsilon_n = -134\,\text{meV}/(n - 0.099)^2. \quad (5)$$

Both found values: 134 meV and -0.099 match their experimentally obtained counterparts (with the aid of Eq. 1) Ry^* =140.5 meV and $\delta = -0.083$.

The applicability range of the formula given by Eq. 1 can be also considered from a different angle, *i.e.*, when it is directly compared/fitted to numerical solutions obtained within the Rytova-Keldysh formalism. As demonstrated in the SM, the validity range of Eq. 1 can be defined with respect to a single, dimensionless parameter of a monolayer structure: $b = a_B^*/r_0^*$, and we find that our simple approach is valid when $b > 0.3$, and estimate that this condition is well satisfied for all monolayers encapsulated in hBN. Nevertheless, even if b is as small as $b \approx 0.1$, what may correspond to the case a monolayer deposited on Si/SiO_2 substrate, the spectrum given by Eq. 1 coincides with that derived with the Rytova-Keldysh potential within the accuracy of 5%.

The model proposed above accounts well for the experimental results obtained for the WSe_2 monolayer and it is interesting to test this model for other S-TMD materials. Unfortunately, the observation of the rich Rydberg spectrum of excitonic states in S-TMD MLs seems to be, so far, uniquely reserved for WSe_2 MLs. Nevertheless, for all other S-TMD MLs studied, *i.e.*, MoS_2, WS_2, and $MoSe_2$ MLs encapsulated in hBN, we observe the $2s$ in addition to the $1s$ excitonic resonance,see Fig. 4 and Fig. S7 in SM. The energy positions, E_{1s} and E_{2s}, of the $1s$ and $2s$ resonances (of A exciton) are directly read from Fig. 4. Of interest is the energy difference $(E_{2s}\text{-}E_{1s}) = \Delta E^{\text{exp}}_{2s-1s}$ listed in Table I, for all four MLs investigated.

As shown in Fig. 4, the PL peaks associated with the excited excitonic states are followed by noticeable PL tails developed at higher energies. We believe that these tails penetrate above the band-gap energies which are, however, not spectacularly marked in the spectra. We note, that in the case of our WSe_2 ML, the PL

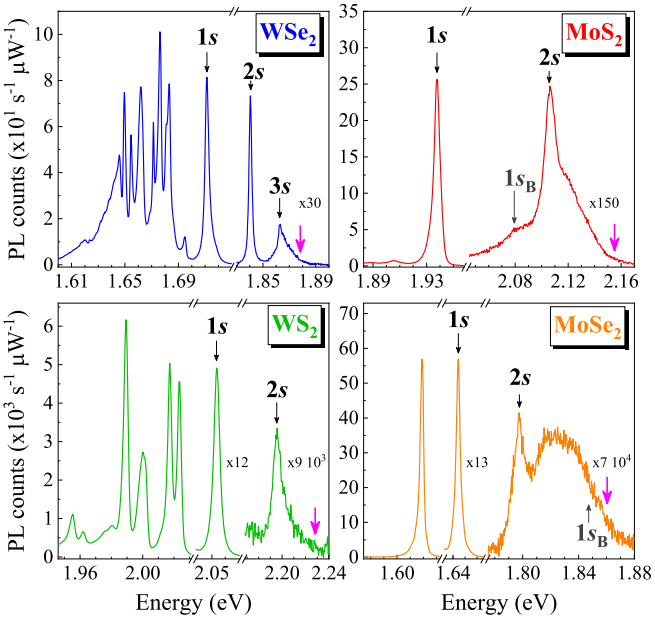

FIG. 4. Low temperature PL spectra of S-TMD MLs at T=5 K. The pink vertical arrows denote the estimated band-gap energies E_g. The chosen spectral regions are scaled for clarity. Typically for S-TMDs monolayers, the most pronounced emission feature seen in our spectra is due to the $1s$ excitonic resonance accompanied by low energy peaks commonly assigned to different excitonic complexes [33, 40, 43–53].

intensity at the band-gap energy (accurately estimated from magneto-PL data and marked with a pink arrow in Fig. 4) consists of 5% of the intensity of the $2s$ exciton PL peak. Applying the same convention to all spectra presented in Fig. 4, we estimate the band gaps in the three other MLs, as illustrated with pink arrows in this figure. Most critical is estimation of the band gap in $MoSe_2$ ML (see SM for details). With estimation of the band gap and reading the energies of $1s$ excitonic resonances directly from the spectra (see Fig. 4), we extract exciton binding energies $E_b^{exp} = (E_g - E_{1s})$ and show their values in Table I. Having estimated $\Delta E^{\text{exp}}_{2s-1s}$ and E_b^{exp} parameters, and following our predictions that $E_{ns} = E_g - Ry^*/(n+\delta)^2$, where $Ry^* = Ry \times \mu/(\varepsilon_{hBN}^2 m_0)$, we

TABLE I. Series of parameters (E_b^{exp}, $\Delta E^{\text{exp}}_{2s-1s}$, δ^{exp}, μ^{exp}) obtained from the analysis of PL spectra shown in Fig.4, compared with results of DFT calculations (μ^{DFT}) [42].

Monolayer	E_b^{exp} (meV)	$\Delta E^{\text{exp}}_{2s-1s}$ (meV)	δ^{exp}	μ^{exp} (m_0)	μ^{DFT} (m_0)
WSe_2	167	130	-0.083	0.21	0.16
$MoSe_2$	216	153	0.174	0.44	0.27
WS_2	174	141	-0.229	0.15	0.15
MoS_2	217	168	-0.095	0.26	0.24

derive the δ^{exp} and μ^{exp} parameters for all MLs studied, see Table I. We found very good agreement between our estimations and results of DFT calculations [42] for the reduced masses in WS_2 and MoS_2 MLs, while we note an apparent discrepancy for WSe_2 and $MoSe_2$ MLs. We also applied our model to estimate values of band gaps and binding energies to the experimental data available in the literature [9, 37], which is discussed in SM.

Concluding, we have demonstrated that the ns Rydberg series of excitonic states in S-TMD monolayers encapsulated in hBN follows a simple energy ladder: $\epsilon_n = -Ry^*/(n+\delta)^2$. $Ry^* = Ry \times \mu/(\varepsilon^2 m_0)$, where Ry is the Rydberg energy, μ denotes the reduced e-h mass, and ε is the dielectric constant of the surrounding material. The dielectric polarizability χ_{2D} of a monolayer is only encoded in δ. Strikingly, δ is found to be close to zero for WSe_2 (and MoS_2) ML whose ϵ_n spectrum resembles that of a 3D hydrogen atom. The proposed model may be applicable to other Coulomb bound states (*e.g.* donor and/or acceptor states), also to other systems, such as colloidal platelets [5] or 2D perovskites [6]. Interestingly, the $\epsilon_n = -Ry^*/(n+\delta)^2$ formula coincides with that expected for a hypothetical hydrogen atom in fractional dimension N, $(N = 2\delta + 3)$, which was indeed speculated [16] to mimic the spectrum of Coulomb bound states in low-dimensional semiconductor structures.

The work has been supported by the EU Graphene Flagship project (no. 785219), the ATOMOPTO project (TEAM programme of the Foundation for Polish Science, co-financed by the EU within the ERD-Fund), the National Science Centre, Poland (grants no. 2013/10/M/ST3/00791, 2017/27/B/ST3/00205, and 2018/31/B/ST3/02111), and the Nanofab facility of the Institut Néel, CNRS UGA, and the LNCMI-CNRS, a member of the European Magnetic Field Laboratory (EMFL). M.B. acknowledges the financial support from the Ministry of Education, Youth and Sports of the Czech Republic under the project CEITEC 2020 (LQ1601). K.W. and T.T. acknowledge support from the Elemental Strategy Initiative conducted by the MEXT, Japan, and the CREST (JPMJCR15F3), JST.

* maciej.molas@fuw.edu.pl
† marek.potemski@lncmi.cnrs.fr

[1] N. S. Rytova, Proc. MSU, Phys. Astron. **3**, 308 (1967).
[2] L. V. Keldysh, JETP Lett. **29**, 658 (1979).
[3] V. N. Kotov, B. Uchoa, V. M. Pereira, F. Guinea, and A. H. Castro Neto, Rev. Mod. Phys. **84**, 1067 (2012).
[4] C. Faugeras, S. Berciaud, P. Leszczynski, Y. Henni, K. Nogajewski, M. Orlita, T. Taniguchi, K. Watanabe, C. Forsythe, P. Kim, R. Jalil, A. K. Geim, D. M. Basko, and M. Potemski, Phys. Rev. Lett. **114**, 126804 (2015).
[5] S. Ithurria, M. D. Tessier, B. Mahler, R. P. S. M. Lobo, and A. L. Dubertret, B.and Efros, Nature Materials **10**, 936 (2011).
[6] C. C. Stoumpos, D. H. Cao, D. J. Clark, J. Young, J. M. Rondinelli, J. I. Jang, J. T. Hupp, and M. G. Kanatzidis, Chemistry of Materials **28**, 2852 (2016).
[7] J.-C. Blancon, A. V. Stier, W. Tsai, H.and Nie, C. C. Stoumpos, B. Traoré, L. Pedesseau, M. Kepenekian, F. Katsutani, G. T. Noe, J. Kono, S. Tretiak, S. A. Crooker, C. Katan, M. G. Kanatzidis, J. J. Crochet, J. Even, and A. D. Mohite, Nature Communications **9**, 2254 (2018).
[8] A. K. Geim and I. Grigorieva, Nature **499**, 419 (2013).
[9] A. Chernikov, T. C. Berkelbach, H. M. Hill, A. Rigosi, Y. Li, O. B. Aslan, D. R. Reichman, M. S. Hybertsen, and T. F. Heinz, Phys. Rev. Lett. **113**, 076802 (2014).
[10] A. Raja, A. Chaves, J. Yu, G. Arefe, H. M. Hill, A. F. Rigosi, T. C. Berkelbach, P. Nagler, C. Schüller, T. Korn, C. Nuckolls, J. Hone, L. E. Brus, T. F. Heinz, D. R. Reichman, and A. Chernikov, Nature Communications **8**, 15251 (2017).
[11] M. Koperski, M. R. Molas, A. Arora, K. Nogajewski, A. Slobodeniuk, C. Faugeras, and M. Potemski, Nanophotonics **6**, 1289 (2017).
[12] G. Wang, A. Chernikov, M. M. Glazov, T. F. Heinz, X. Marie, T. Amand, and B. Urbaszek, Rev. Mod. Phys. **90**, 021001 (2018).
[13] M. Trushin, M. O. Goerbig, and W. Belzig, Phys. Rev. Lett. **120**, 187401 (2018).
[14] A. H. MacDonald and D. S. Ritchie, Phys. Rev. B **33**, 8336 (1986).
[15] E. S. Koteles and J. Y. Chi, Phys. Rev. B **37**, 6332 (1988).
[16] P. Christol, P. Lefebvre, and H. Mathieu, Journal of Applied Physics **74**, 5626 (1993).
[17] A. Kratzer, Zeitschrift für Physik **3**, 289 (1920).
[18] O. Akimoto and H. Hasegawa, Journal of the Physical Society of Japan **22**, 181 (1967).
[19] M. Potemski, L. Viña, G. E. W. Bauer, J. C. Maan, K. Ploog, and G. Weimann, Phys. Rev. B **43**, 14707 (1991).
[20] See Supplemental Material [url] for description of the experimental details, analysis of an excitonic spectrum in the Kratzer and Rytova-Keldysh potentials, and additional experimental results comprising magneto-photoluminescence and low temperature reectance contrast spectra of the investigated monolayers, which includes Refs. [1,2,9,16,17,21-37].
[21] A. Castellanos-Gomez, M. Buscema, R. Molenaar, V. Singh, L. Janssen, H. S. J. van der Zant, and G. A. Steele, 2D Materials **1**, 011002 (2014).
[22] X. L. Yang, S. H. Guo, F. T. Chan, K. W. Wong, and W. Y. Ching, Phys. Rev. A **43**, 1186 (1991).
[23] H. A. Bethe and E. M. Salpeter, *Quantum mechanics of one and two-electron atoms* (Springer-Verlag Berlin, 1957).
[24] A. V. Stier, N. P. Wilson, K. A. Velizhanin, J. Kono, X. Xu, and S. A. Crooker, Phys. Rev. Lett. **120**, 057405 (2018).
[25] T. C. Berkelbach, M. S. Hybertsen, and D. R. Reichman, Phys. Rev. B **88**, 045318 (2013).
[26] H. Bateman and A. Erdelyi, *Higher Transcendental Functions, Volume 1* (Mc Graw-Hill book Co. New York, 1953).
[27] R. Geick, C. H. Perry, and G. Rupprecht, Phys. Rev. **146**, 543 (1966).
[28] P. Cudazzo, I. V. Tokatly, and A. Rubio,

Phys. Rev. B **84**, 085406 (2011).
[29] Y. Li, A. Chernikov, X. Zhang, A. Rigosi, H. M. Hill, A. M. van der Zande, D. A. Chenet, E.-M. Shih, J. Hone, and T. F. Heinz, Phys. Rev. B **90**, 205422 (2014).
[30] A. Arora, M. Koperski, K. Nogajewski, J. Marcus, C. Faugeras, and M. Potemski, Nanoscale **7**, 10421 (2015).
[31] A. Arora, K. Nogajewski, M. Molas, M. Koperski, and M. Potemski, Nanoscale **7**, 20769 (2015).
[32] M. R. Molas, K. Nogajewski, A. O. Slobodeniuk, J. Binder, M. Bartos, and M. Potemski, Nanoscale **9**, 13128 (2017).
[33] C. Robert, M. A. Semina, F. Cadiz, M. Manca, E. Courtade, T. Taniguchi, K. Watanabe, H. Cai, S. Tongay, B. Lassagne, P. Renucci, T. Amand, X. Marie, M. M. Glazov, and B. Urbaszek, Phys. Rev. Materials **2**, 011001 (2018).
[34] B. Han, C. Robert, E. Courtade, M. Manca, S. Shree, T. Amand, P. Renucci, T. Taniguchi, K. Watanabe, X. Marie, L. E. Golub, M. M. Glazov, and B. Urbaszek, Phys. Rev. X **8**, 031073 (2018).
[35] A. O. Slobodeniuk, Ł. Bala, M. Koperski, M. R. Molas, P. Kossacki, K. Nogajewski, M. Bartos, K. Watanabe, T. Taniguchi, C. Faugeras, and M. Potemski, 2D Materials **6**, 025026 (2019).
[36] I. C. Gerber, E. Courtade, S. Shree, C. Robert, T. Taniguchi, K. Watanabe, A. Balocchi, P. Renucci, D. Lagarde, X. Marie, and B. Urbaszek, Phys. Rev. B **99**, 035443 (2019).
[37] M. Goryca, J. Li, A. V. Stier, S. A. Crooker, T. Taniguchi, K. Watanabe, E. Courtade, S. Shree, C. Robert, B. Urbaszek, and X. Marie, arXiv e-prints , arXiv:1904.03238 (2019), arXiv:1904.03238 [cond-mat.mes-hall].
[38] M. Manca, M. M. Glazov, C. Robert, F. Cadiz, T. Taniguchi, K. Watanabe, E. Courtade, T. Amand, P. Renucci, X. Marie, G. Wang, and B. Urbaszek, Nature Communications **8**, 14927 (2017).
[39] C. M. Chow, H. Yu, A. M. Jones, J. Yan, D. G. Mandrus, T. Taniguchi, K. Watanabe, W. Yao, and X. Xu, Nano Letters **17**, 1194 (2017).
[40] S.-Y. Chen, T. Goldstein, J. Tong, T. Taniguchi, K. Watanabe, and J. Yan, Phys. Rev. Lett. **120**, 046402 (2018).
[41] E. Liu, J. van Baren, T. Taniguchi, K. Watanabe, Y.-C. Chang, and C. H. Lui, Phys. Rev. B **99**, 205420 (2019).
[42] A. Kormányos, G. Burkard, M. Gmitra, J. Fabian, V. Zólyomi, N. D. Drummond, and V. Fal'ko, 2D Materials **2**, 022001 (2015).
[43] F. Cadiz, E. Courtade, C. Robert, G. Wang, Y. Shen, H. Cai, T. Taniguchi, K. Watanabe, H. Carrere, D. Lagarde, M. Manca, T. Amand, P. Renucci, S. Tongay, X. Marie, and B. Urbaszek, Phys. Rev. X **7**, 021026 (2017).
[44] J. Wierzbowski, J. Klein, F. Sigger, C. Straubinger, M. Kremser, T. Taniguchi, K. Watanabe, U. Wurstbauer, A. W. Holleitner, M. Kaniber, K. Müller, and J. J. Finley, Scientific Reports **7**, 12383 (2017).
[45] E. Courtade, M. Semina, M. Manca, M. M. Glazov, C. Robert, F. Cadiz, G. Wang, T. Taniguchi, K. Watanabe, M. Pierre, W. Escoffier, E. L. Ivchenko, P. Renucci, X. Marie, T. Amand, and B. Urbaszek, Phys. Rev. B **96**, 085302 (2017).
[46] C. Robert, T. Amand, F. Cadiz, D. Lagarde, E. Courtade, M. Manca, T. Taniguchi, K. Watanabe, B. Urbaszek, and X. Marie, Phys. Rev. B **96**, 155423 (2017).
[47] D. Vaclavkova, J. Wyzula, K. Nogajewski, M. Bartos, A. O. Slobodeniuk, C. Faugeras, M. Potemski, and M. R. Molas, Nanotechnology **29**, 325705 (2018).
[48] P. Nagler, M. V. Ballottin, A. A. Mitioglu, M. V. Durnev, T. Taniguchi, K. Watanabe, A. Chernikov, C. Schüller, M. M. Glazov, P. C. M. Christianen, and T. Korn, Phys. Rev. Lett. **121**, 057402 (2018).
[49] M. Barbone, A. R. P. Montblanch, D. M. Kara, C. Palacios-Berraquero, A. R. Cadore, D. De Fazio, B. Pingault, E. Mostaani, H. Li, B. Chen, K. Watanabe, T. Taniguchi, S. Tongay, G. Wang, A. C. Ferrari, and M. Atatüre, Nature Communications **9**, 3721 (2018).
[50] S.-Y. Chen, T. Goldstein, T. Taniguchi, K. Watanabe, and J. Yan, Nature Communications **9**, 3717 (2018).
[51] Z. Li, T. Wang, Z. Lu, C. Jin, Y. Chen, Y. Meng, Z. Lian, T. Taniguchi, K. Watanabe, S. Zhang, D. Smirnov, and S.-F. Shi, Nature Communications **9**, 3719 (2018).
[52] M. Molas, A. Slobodeniuk, T. Kazimierczuk, K. Nogajewski, M. Bartos, P. Kapuściński, K. Oreszczuk, K. Watanabe, T. Taniguchi, C. Faugeras, P. Kossacki, D. Basko, and M. Potemski, Phys. Rev. Lett. **123**, 096803 (2019).
[53] E. Liu, J. van Baren, Z. Lu, M. M. Altaiary, T. Taniguchi, K. Watanabe, D. Smirnov, and C. H. Lui, Phys. Rev. Lett. **123**, 027401 (2019).